Magnetization in molecular iron rings

B. Normand,[1,2] X. Wang,[3,4,5] X. Zotos,[3] and Daniel Loss[2]
[1]*Theoretische Physik III, Elektronische Korrelationen und Magnetismus, Institut für Physik, Universität Augsburg, D-86135 Augsburg, Germany*
[2]*Departement für Physik und Astronomie, Universität Basel, CH-4056 Basel, Switzerland*
[3]*Institut Romand de Recherche Numérique en Physique des Materiaux (IRRMA), PPH-Ecublens, CH-1015 Lausanne, Switzerland*
[4]*Max-Planck-Institut für Physik Komplexer Systeme, Nöthnitzerstraβe 38, D-01187 Dresden, Germany*
[5]*Institute of Theoretical Physics, Chinese Academy of Sciences, P.O. Box 2735, Beijing 100080, People's Republic of China*
(Received 23 November 2000; published 18 April 2001)

The organometallic ring molecules Fe_6 and Fe_{10} are leading examples of a class of nanoscopic molecular magnets which have been of intense recent interest both for their intrinsic magnetic properties and as candidates for the observation of macroscopic quantum coherent phenomena. Torque magnetometry experiments have been performed to measure the magnetization in single crystals of both systems. We provide a detailed interpretation of these results, with a view to full characterization of the material parameters. We present both the most accurate numerical simulations performed to date for ring molecules, using exact diagonalization and density-matrix renormalization-group techniques, and a semiclassical description for purposes of comparison. The results permit quantitative analysis of the variation of critical fields with angle, of the nature and height of magnetization and torque steps, and of the width and rounding of the plateau regions in both quantities.

DOI: 10.1103/PhysRevB.63.184409 PACS number(s): 75.10.Jm, 03.65.Sq, 73.40.Gk, 75.30.Gw

I. INTRODUCTION

The molecular iron ring, or ''ferric wheel'' systems Fe_6 and Fe_{10} (Ref. 1) present an interesting subgroup of magnetic molecular clusters. Both materials have dominant antiferromagnetic (AF) coupling between spins $S=\frac{5}{2}$ on each iron site and have a ground state of total spin $S=0$. The magnetic properties of such nanoscopic molecules result from the interplay of superexchange interactions between the atomic spins, dipolar coupling of the local moments, and on-site spin anisotropies arising from ligand configurations. In view of these complexities, and of the possibilities which exist[2] to influence the relative strengths of each interaction type through the non-Fe constituents of the molecules, a detailed understanding of the magnetic response is crucial. In appropriate parameter regimes, the ring systems are considered[3,4] to be candidates for the observation of ''macroscopic'' quantum phenomena, in the form of quantum coherent tunneling of the Néel vector.

The magnetization $M(B)$ of single crystals of both Fe_6 and Fe_{10} has recently been studied experimentally by cantilever torque magnetometry,[5] using magnetic fields up to 23 T and at temperatures down to 0.45 K. In the Fe_6 system, a selection of materials is available:[2] for Na:Fe_6 only the first magnetization step to the $S=1$ state and at the field $B_{c1} \simeq 17$ T is accessible; for Li:Fe_6, $B_{c2} \simeq 21$ T is also observed. For Fe_{10}, the fields B_{c1}–B_{c4}, corresponding to the lowest four magnetization steps, may be measured. In a very recent analysis[6] of Na:Fe_6, temperatures as low as 30 mK were probed, and a temperature independence of the step width was observed, a result to which we will return later. In each material, B_{c1} is found to be largest in the orientation where the magnetic field is applied along the axes of the rings (which we will denote as $\psi=0$), and smallest when the field is directed in the plane of the rings ($\psi=\pi/2$). The variation between these extrema is to a good approximation a sinusoidal function of 2ψ.

Here we present a detailed analysis of the magnetization in these ferric wheels, considering the spacing and widths of the magnetization steps, the flatness of the plateaus, and the angular variation of the critical fields. The primary results are given by numerical simulations: we perform both a Lanczos diagonalization of the full Fe_6 system, and density-matrix renormalization-group (DMRG) studies of finite $S=\frac{5}{2}$ systems. Both techniques are exact at zero temperature for six-site rings, and DMRG studies give highly accurate results also for the 10-site case. As an aid to interpretation, we appeal in Sec. II to a semiclassical formulation for the molecular spin as a rigid-rotor model and for the low-energy dynamics of the Néel vector.[4] In Sec. III we compare this model with existing magnetization data to extract the relevant materials parameters. In Sec. IV we present the numerical simulations, and in Sec. V we discuss the qualitative and quantitative significance of the results. Sec. VI contains a summary and conclusions.

II. ANALYTICAL DESCRIPTION

We begin by considering a semiclassical description for the behavior of magnetic molecular rings in order to deduce approximate materials parameters for the simulations. Justification for the applicability of the semiclassical model may be found in Ref. 4. The minimal starting Hamiltonian for the ring system shown schematically in Fig. 1 is

$$H=J\sum_{i=1}^{N}\mathbf{S}_i\cdot\mathbf{S}_{i+1}+\sum_{i=1}^{N}U_i(\mathbf{S}_i)+\hbar\mathbf{h}\cdot\sum_{i=1}^{N}\mathbf{S}_i, \qquad (1)$$

where $N=6$ or 10, $\mathbf{S}_1=\mathbf{S}_{N+1}$, and $\mathbf{h}=g\mu_B\mathbf{B}/\hbar$. J is the dominant superexchange interaction which enforces an AF spin configuration around the ring, U contains intraring di-

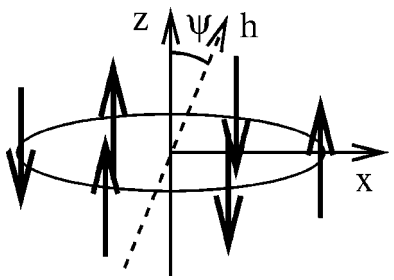

FIG. 1. Schematic representation of Fe_6 ring at zero field, showing spins aligned along easy axis of orientation normal to ring plane. Also shown is arbitrary axis of magnetic field alignment.

polar interactions and single-ion anisotropy terms, and the final term is the Zeeman coupling. For a ring geometry, it is easy to show that dipolar interactions within a single molecule contribute only an effective easy-axis spin anisotropy which favors the axis normal to the ring plane. In addition, the environment of each Fe ion due to the surrounding ligand groups in general has a noncubic point-group symmetry; for the majority of cases the on-site symmetry may be taken as uniaxial, and, again with the assistance of the ring geometry which allows[4] radial anisotropy to be subsumed within the uniaxial terms, we will assume this form of anisotropy. In all systems known to date, this has been found to be weak, and of easy-axis orientation in the same sense as above. Thus to a reasonable approximation, the separate contributions to the U term may be combined as a single, effective on-site anisotropy term $\Sigma_{i=1}^{N} -k_z S_{i,z}^2$, in which the sign of k_z is chosen such that a positive value implies an easy axis for the orientation of the local spins. In Ref. 2 it was shown that the dipolar and single-site components of the effective k_z may be attributed separately. We consider an arbitrary magnetic-field alignment, parametrized by the angle ψ to the easy axis in the (x,z) plane. The field acts as an effective hard axis for an AF system and causes spin reorientation for angles $\psi \neq \pi/2$.

The Hamiltonian (1) is mapped[4] to a form of nonlinear σ model for the staggered magnetization $\mathbf{n}$, by expressing the spins $\mathbf{S}_i$ in coherent-state representation as $S\mathbf{\Omega}_i = (-1)^i S\mathbf{n}_i + \mathbf{l}_i$, and integrating over the uniform component $\mathbf{l}$. One obtains

$$\mathcal{L}_E = N\left\{\frac{\hbar^2}{8J}[\dot{\mathbf{n}}^2 + i\mathbf{h}\cdot(\mathbf{n}\wedge\dot{\mathbf{n}}) - [h^2 - (\mathbf{h}\cdot\mathbf{n})^2]] - k_z S^2 n_z^2\right\}. \tag{2}$$

Gradient terms $(\partial_x \mathbf{n})^2$, where x is the spatial coordinate around the ring, may be neglected for small N, because for a small, closed system such as the ring geometry they represent significantly higher-lying energy states. This semiclassical description of the low-energy physics is also suitable for analyzing quantum coherence effects.[4]

The Hamiltonian formulation canonically conjugate to $\mathcal{L}_E$ (2) is deduced by considering the continuous spatial variable $\mathbf{x} = R\mathbf{n}$, its conjugate momentum $\mathbf{p} = \partial\mathcal{L}_E/\partial\dot{\mathbf{x}}$, and the angular momentum $\mathbf{L} = \mathbf{x}\wedge\mathbf{p}$. In real time $t = -i\tau$ this is

$$H = \frac{2J}{N\hbar^2}\mathbf{L}^2 + \mathbf{h}\cdot\mathbf{L} - Nk_z S^2 n_z^2, \tag{3}$$

which may be divided in obvious notation into $H_0(\mathbf{L}) + H_A$, the latter term denoting the anisotropy contribution. H_0 has eigenstates $|L,L_z\rangle = |l,m\rangle$ with $l = 0,1,2,\ldots$ and $-l \leq m \leq l$, and eigenvalues $E_{l,m} = (2J/N)l(l+1) + g\mu_B Bm$. The energy spectrum is shown as a function of applied field in Fig. 6 of Ref. 5. Thus H_0 describes a staircaselike magnetization with steps occurring at the field values $B_{cn} = 4Jn/g\mu_B N$, where $n = 1,2,3,\ldots$ is an integer. This behavior accounts directly for the gross features of the observed magnetization curves.[5] Inclusion of the anisotropy term H_A allows one to proceed to the effective spin Hamiltonian[7] employed in Ref. 5, and to a discussion of the variation of the critical fields $B_{cn}(\psi)$ with angle. In practice, this is used to deduce the anisotropy parameter k_z. In the presence of a single-ion anisotropy, the energy levels at zero field of the first (triplet) excitations are not degenerate, and B_{c1} is given by the field where the $m = -1$ level crosses the singlet. Note that in contrast to Fig. 1, we now take the field axis to define $\hat{z}$ and rotate the ring by angle ψ in the (x,z) plane. For arbitrary ψ, the anisotropy term takes the form

$$\begin{aligned} H_A &= -Nk_z S^2 \cos^2\psi n_z^2 - Nk_z S^2 \sin^2\psi n_x^2, \\ &= -Nk_z S^2(\cos^2\theta\cos^2\psi + \sin^2\theta\sin^2\phi\sin^2\psi), \end{aligned} \tag{4}$$

which describes simply the fact that components n_z and n_x profit from the easy axis as the ring is tilted relative to the field. θ and ϕ are, respectively, the axial and azimuthal polar coordinates respectively. The eigenvalues E_A are evaluated using the spherical harmonic wave functions $Y_{l,m}(\theta,\phi)$. The results for the singlet and triplet levels are

$$\begin{aligned} E_{0,0} &= -\frac{1}{3}Nk_z S^2(\cos^2\psi + \sin^2\psi) = -\frac{1}{3}Nk_z S^2, \\ E_{1,0} &= \frac{4J}{N} - \frac{3}{5}Nk_z S^2\cos^2\psi - \frac{1}{5}Nk_z S^2\sin^2\psi, \\ E_{1,\pm1} &= \frac{4J}{N} - \frac{1}{5}Nk_z S^2\cos^2\psi - \frac{2}{5}Nk_z S^2\sin^2\psi \pm g\mu_B B. \end{aligned} \tag{5}$$

Comparison of $E_{0,0}$ with $E_{1,-1}$ gives the result

$$B_{c1} = \frac{4J}{g\mu_B N}\left[1 + \frac{k_z N^2 S^2}{30J}\left(1 - \frac{3}{2}\sin^2\psi\right)\right], \tag{6}$$

and thus a clear demonstration that the angle dependence observed in both ferric wheel systems corresponds to an easy-axis anisotropy for the spin direction in the original model. For future reference, we define as $B_{c1}^0 = 4J/g\mu_B N$ the field value where the $S = 0 \rightarrow 1$ transition would occur in the absence of magnetic anisotropy, whence Eq. (6) may be re-expressed as

$$B_{c1} = B_{c1}^0\left[1 + \frac{1}{15}\lambda_{c1}\left(1 - \frac{3}{2}\sin^2\psi\right)\right], \tag{7}$$

where λ_{c1} is the value of the anisotropy-field ratio[4] $\lambda = 8k_zJS^2/(g\mu_B B)^2$ at $B=B^0_{c1}$. Finally, by following the same procedure as in Eq. (5) for the wave function $Y_{2,-2}(\theta,\phi)$, one obtains

$$E_{2,-2}=\frac{12J}{N}-\frac{1}{7}Nk_zS^2\cos^2\psi-\frac{3}{7}Nk_zS^2\sin^2\psi-2g\mu_BB, \tag{8}$$

and thus

$$B_{c2}=2B^0_{c1}\left[1+\frac{1}{70}\lambda_{c1}\left(1-\frac{3}{2}\sin^2\psi\right)\right]. \tag{9}$$

It is evident that in the presence of anisotropy, the widths of the magnetization steps are no longer equal.

Before leaving the rigid-rotor model [Eq. (3)], we may employ it to make a valuable qualitative observation concerning the nature of the magnetization. The situation of most interest for quantum transitions between low-energy states of similar energy is when the field is applied perpendicular to the axis of the anisotropy. In the real materials, this anisotropy is rather weak, and it would be most appropriate to seek quantum coherent phenomena in the high-field regime of Ref. 4. If the field is dominant and sets the quantization axis ($\hat{z}$) of the rotor, the on-site anisotropy term takes the form $-\Sigma_i k_z S_x^2 = -\frac{1}{4}\Sigma_i k_z (S_+ + S_-)^2$, where S_α is a spin operator acting within the $S=\frac{5}{2}$ manifold on each site. The anisotropy, considered as a perturbation, may change the total-spin state of the system only by $\Delta S=0,\pm 2$. All level crossings between eigenstates of the rigid rotor will then be true crossings when $\Delta m=\pm 1,\pm 3,\ldots$ but will become anticrossings due to the mixing perturbation when $\Delta m=\pm 2$, $\pm 4,\ldots$ Because the ground-state level alterations always involve $\Delta m=1$, we thus obtain a simple understanding for the fact that all of the magnetization steps will have vertical portions for the starting Hamiltonian (1), whereas the energy-level splitting $E_{01}=E_1-E_0$ will be not a sawtooth-shaped function but a rounded one.[4] In principle, the anisotropy term may be reexpressed in terms of linear combinations of operators L_α for the rigid rotor, allowing one to obtain analytical expressions for the numerical results to follow.

III. EXPERIMENTAL COMPARISON

The results of the previous section may be applied directly to the experimental data of Refs. 5 and 2. The variation of the critical fields for the lowest magnetization steps with the angle ψ between the applied field and the ring axis has been measured to high accuracy by torque magnetometry, and is presented in Fig. 4 of Ref. 5 for Na:Fe_6 and Fe_{10}, and in Fig. 3 of Ref. 2 for Li:Fe_6. The mean value of the field at which the step occurs gives the antiferromagnetic superexchange coupling J, which is responsible for maintaining the $S=0$ ground-state spin configuration at zero field. The variation of the critical-field values B_c between their extrema at $\psi=0$ and $\psi=\pi/2$ gives the effective anisotropy parameter k_z for each material. In the case of Li:Fe_6, the two steps which have been characterized give an independent verification of the consistency of the rigid-rotor description over a wider field range.

TABLE I. Critical field for first magnetization step B^0_{c1}; deduced value of superexchange J; maximum critical-field variation ΔB_c; deduced value of effective, single-ion anisotropy k_z; offset angle θ for Fe_6 and Fe_{10} materials. Data taken from Refs. 5 and 2.

	B^0_{c1} (T)	J(K)	ΔB_c (T)	k_z/J	θ
Na:Fe_6	16.32	32.77	2.49T	0.0136	0.025
Fe_{10}	4.65	15.56	1.28T	0.0088	−0.305
Li:Fe_6	10.38	20.83	0.620	0.0053	0.011
Li:Fe_6	10.30	20.68	0.328	0.0066	−0.091

Fits of the data to Eqs. (6) or (7) for the first steps, and to Eq. (9) for the second step in Li:Fe_6, yield the values of J and k_z shown in Table I. The parameters in the last row are taken from B_{c2} for Li:Fe_6 and show quite satisfactory consistency with the values deduced from the first step. The results are illustrated in Figs. 2 and 3. The angular offset in the final column of the table is an alignment parameter concerning the experimental orientations of crystal and goniometer and is not important for the intrinsic physics. This angle is quite large in Fe_{10} [Fig. 2(b)], where the crystal structure contains rings of two different orientations, that are

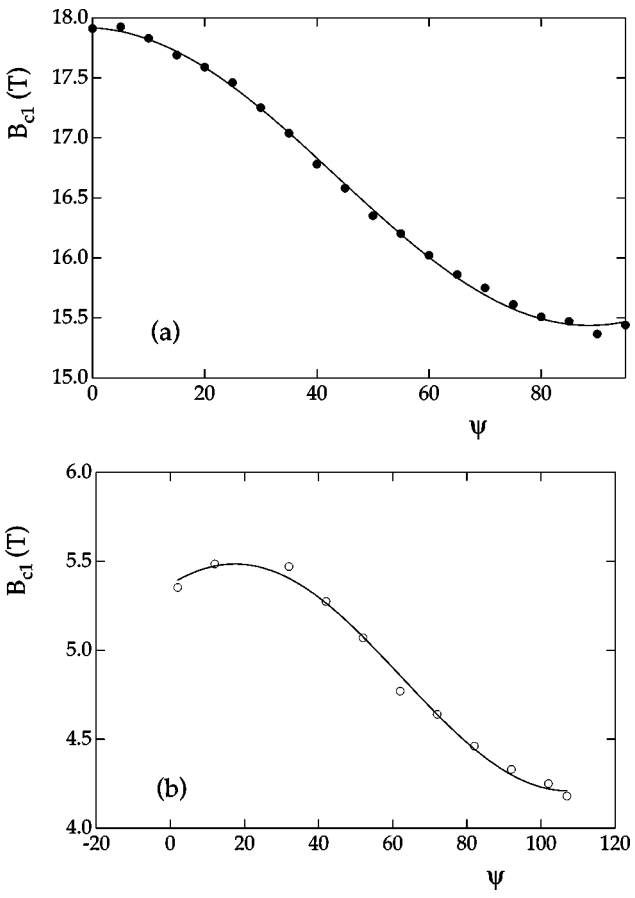

FIG. 2. Angular variation of critical field B_{c1} for first magnetization step in (a) Na:Fe_6 and (b) Fe_{10}. Data points are from Ref. 5, and solid lines are fits using Eq. (6) with the parameters in the table.

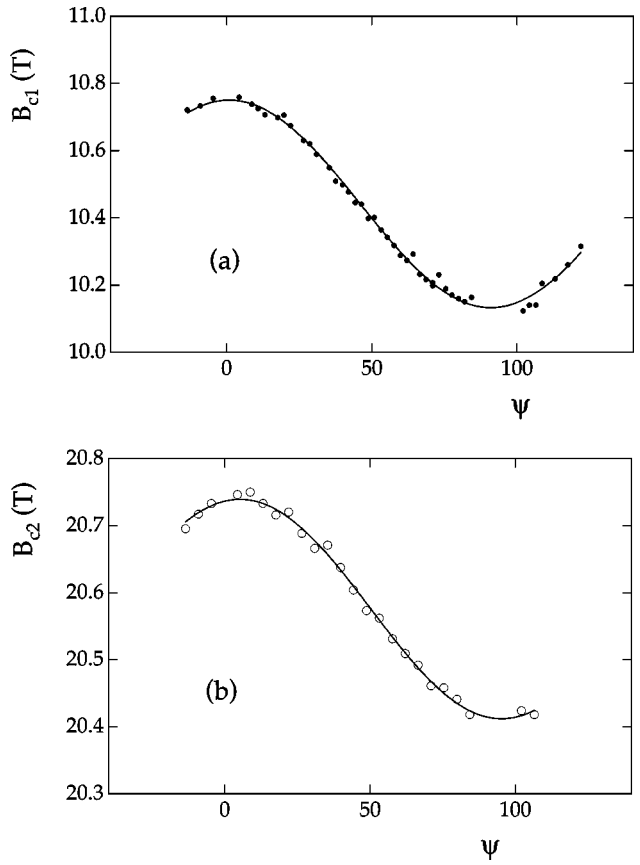

FIG. 3. Angular variation of critical fields B_{c1} (a) and B_{c2} (b) in Li:Fe_6. Data points are from Ref. 2, and solid lines are fits using Eqs. (6) and (9) with the parameters in the table.

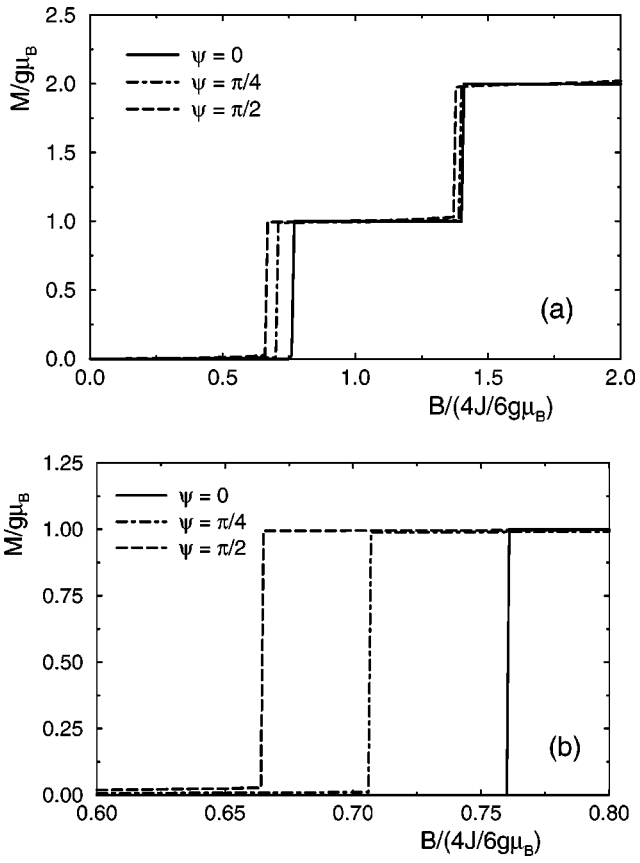

FIG. 4. (a) Magnetization $M(B)$ for Na:Fe_6 from ED for field angles $\psi=0$, $\pi/4$, and $\pi/2$. (b) Magnification of $S=0\rightarrow1$ step region, illustrating anisotropy-induced variation in B_{c1} and vertical nature of step.-

observed[5] in the same projection on the field direction.

Although the ratios k_z/J are rather small, being at most on the order of 1%, we note that the definition of the terms in Eqs. (2) and (3) includes a factor of S^2. Comparison of $\Delta B_c/2$ with B_{c1}^0 gives a more realistic reflection of the effective anisotropy term as an energetic effect on the order of 10%. The fitting procedure employed here bypasses the definition of an intermediate, effective model with parameters D_i; the results of Table I agree well with those of the original works,[5,2] which were extracted by different methods and with the only other known torque measurements.[8] They are also fully consistent with the energy scales deduced from analyses of low-temperature specific heat for Na:Fe_6 and Fe_{10} (Ref. 9) and additionally for Li:Fe_6.[10] The value of k_z/J for Fe_{10} is significantly smaller than that obtained in Ref. 4 based on earlier information.

IV. NUMERICAL SIMULATIONS

With this semiclassical background for the leading-order effects, we turn now to fully quantum-mechanical simulations of the model (1), with the minimal, uniaxial form of the U term

$$H=J\sum_{i=1}^{N}\mathbf{S}_i\cdot\mathbf{S}_{i+1}-\sum_{i=1}^{N}k_zS_{i,z}^2+\hbar\mathbf{h}\cdot\sum_{i=1}^{N}\mathbf{S}_i. \qquad (10)$$

We work with arbitrary field angle and strength and with focus on the experimental parameter regimes for Na:Fe_6 and Fe_{10} (Table I).

A. Exact diagonalization

For Fe_6, $N=6$ spins $S=\frac{5}{2}$ require dealing with $(2S+1)^N=46\,656$ basis states. This Hamiltonian matrix is eminently accessible by the Lanczos exact diagonalization (ED) technique, which provides the lowest eigenvalues and their corresponding eigenstates. For any angle of the field to the ring plane, the magnetization is given by

$$M=\frac{\partial E}{\partial B}=\langle S_z\rangle\cos\psi+\langle S_x\rangle\sin\psi, \qquad (11)$$

where $\langle S_\alpha\rangle=\Sigma_{i=1}^{N}\langle S_{i,\alpha}\rangle$ is the ground-state expectation value of component α of the total-spin operator. The results are shown in Fig. 4(a) for Fe_6, with $k_z^{\mathrm{Na}}=0.0136J$, and for angles $\psi=0$, $\pi/4$, and $\pi/2$. The magnetization displays clearly the stepped form, with the step position varying as a function of field angle, which is observed in experiment and expected from the rigid-rotor model (3) of Sec. II. From the location of the steps in field at each angle, we find that the model [Eqs. (7) and (9)] is in quantitative agreement with simulations at the 3–5% level. Given its inherent approxima-

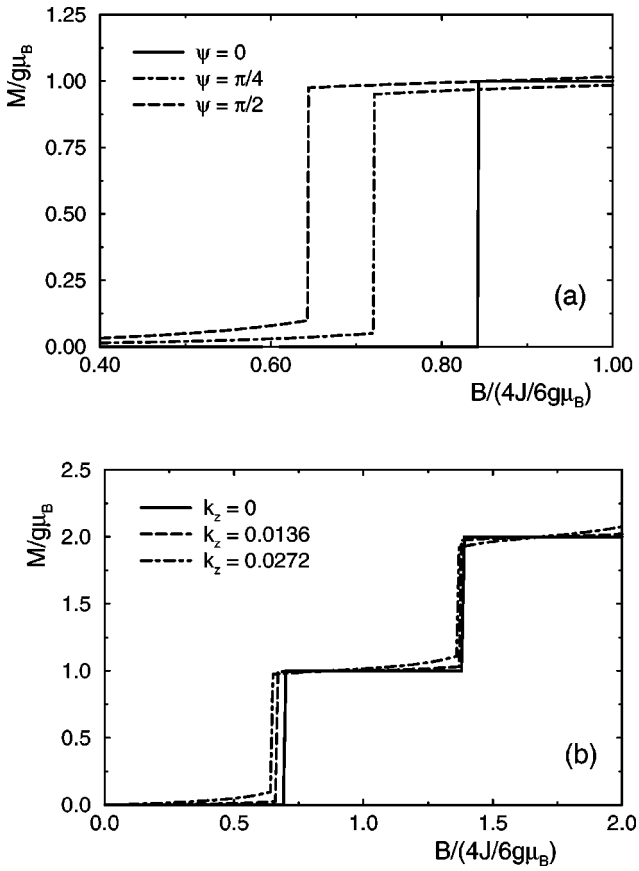

FIG. 5. Magnetization $M(B)$ for an Fe_6 ring from ED (a) for field angles $\psi=0$, $\pi/4$, and $\pi/2$ at anisotropy $k_z=0.0272$ (twice that in Na:Fe_6), and (b) with field angle $\psi=\pi/2$ and anisotropy values $k_z=0$, k_z^{Na}, and $2k_z^{\mathrm{Na}}$.

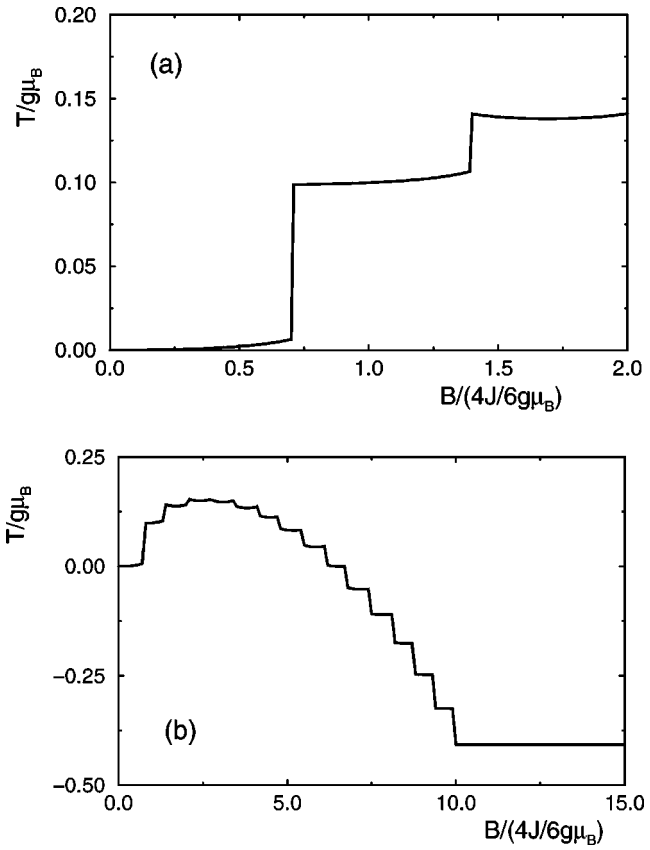

FIG. 6. Torque curve of Na:Fe_6 for $\psi=\pi/4$. (a) Detail at low fields; (b) full field range.

tions, the rigid-rotor description is remarkably satisfactory in the experimentally relevant regime of weak anisotropy which is considered here.

The field resolution in these simulations was 0.001 at the steps in the units given. One observes that the magnetization steps are vertical, as shown in Fig. 4(b) around the first step. However, for angles $\psi\neq 0$ they do not have the full height $\Delta M=1$. This feature, and the curvature of the magnetization ''plateaus,'' are illustrated more clearly in Fig. 5(a) for the same angles, but with the anisotropy taken as $k_z=2k_z^{\mathrm{Na}}$. They may be understood as a natural consequence of zero-point transitions between the energy levels of different spin sectors S_z allowed by the Hamiltonian (10) and are most clearly visible in the magnetization close to the step fields B_{cn}. These are enhanced over a broader region of field around any step B_{cn} as the field angle approaches $\psi=\pi/2$, and the system realizes more closely the optimal geometry[4] of two degenerate spin states corresponding to the Néel vector **n** lying along $\pm\hat{z}$. Fig. 5(b) shows the magnetization curve for geometry $\psi=\pi/2$ for three anisotropy values $k_z=0$, k_z^{Na}, and $2k_z^{\mathrm{Na}}$. It is clear that in the absence of the on-site anisotropy term no quantum transitions may occur, because the Hamiltonian offers no mixing terms. Deviations of the critical fields from their unperturbed values B_{cn}^0, and also the rounding of the plateaus, increase strongly with k_z. Plateau rounding effects are contained in the semiclassical theory[4] and may be compared at the qualitative level.

In Fig. 6(a) is shown the low-field torque

$$T_y=-g\mu_B B(\langle S_x\rangle\cos\psi-\langle S_z\rangle\sin\psi). \tag{12}$$

For the geometry $\psi=\pi/4$ (illustrated), where the torque is maximal, it takes the form of a simple difference between the x and z spin components. As shown in Fig. 6(b), at higher fields this quantity is maximal around the fourth plateau, then decreases, changes sign, and adopts a negative constant value beyond saturation at the 15th plateau. Such behavior may be understood from the asymmetric field evolution of the spin components in the presence of a finite easy-axis anisotropy benefiting one of them. The torque curve, which is directly experimentally accessible, is thus characterized by vertical steps at the magnetization jumps, doubly rounded plateaus, and a distinctive variation in step heights. The first two features may be expected to be visible at the lowest temperatures available in Fe_6 systems, but the evolution of step heights would be hard to measure because of the high fields involved.

B. Density-matrix renormalization group

The DMRG technique[11] is a powerful method for simulating the low-energy properties of one-dimensional systems, which can be much larger than those accessible by ED. Its extensions to periodic systems and to high spins such as S

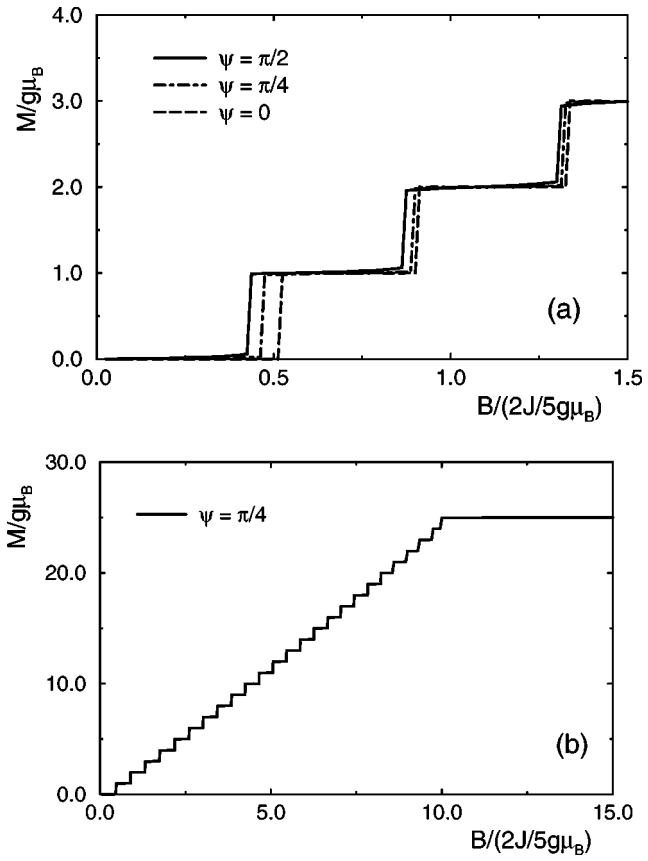

FIG. 7. (a) Magnetization $M(B)$ for Fe_{10} from DMRG for field angles $\psi=0$, $\pi/4$, and $\pi/2$. (b) $M(B)$ for field angle $\pi/4$ over the full field range, illustrating the 25 steps to saturation.

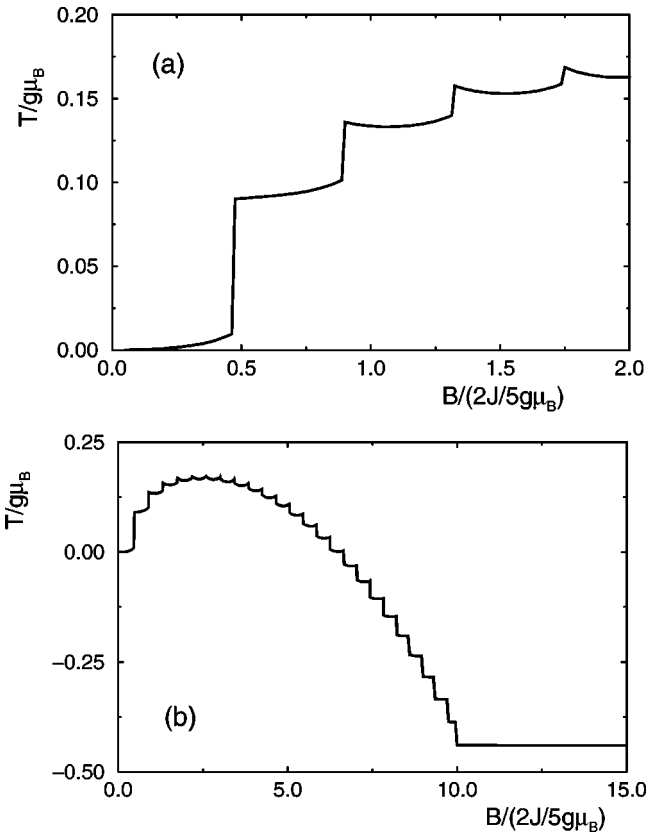

FIG. 8. Torque curve of Fe_{10} for $\psi=\pi/4$. (a) Detail at low fields; (b) full field range.

$=\frac{5}{2}$ are conceptually straightforward, but require considerable numerical effort due to the large spin degree of freedom and, for anisotropic ring systems in a field, the absence of symmetries. In our numerical calculations, we retain at least 80 states and use a finite-size algorithm with 3–5 sweeps for each case. With these conditions, the results are altered by less than 1 part in 10^3 on adding more states or more sweeps. We present here the first results of simulations of this kind (Figs. 7 and 8). As for the ED results above, these are $T=0$ data and show essentially the exact magnetization and torque response of 10-site rings for the minimal model of Eq. (1). Because the DMRG method applied to a sufficiently small system (up to eight sites) involves a very similar truncation to Lanczos ED, the results of simulations on $Na:Fe_6$ are identical to Figs. 4–6; this provides a useful check of both techniques, and obviates further discussion of this system by DMRG.

Figure 7 shows the magnetization curve of Fe_{10} for the physical parameter value $k_z^{10}=0.0088$. The qualitative features of step location and plateau rounding with angles which are visible in the first three steps [Fig. 7(a)] are as in Figs. 4 and 5. Their relative sizes are similar to $Na:Fe_6$ because the smaller value of k_z is offset by the larger value of N. Indeed, the plateau rounding at $\psi=\pi/2$ is found to be more pronounced for Fe_{10} than for $Na:Fe_6$, while, as emphasized above, the step remains vertical; the field increment in Fig. 7(a) is 0.0125 in the units displayed. Fig. 7(b) shows the magnetization response at high fields, which has 25 steps corresponding to the S_z manifolds available between zero and full saturation.

Fig. 8 illustrates the torque for Fe_{10} at $\psi=\pi/4$. The qualitative similarity between Fig. 8(a) and the data of Ref. 5 for the evolution of step heights is worthy of note, although the data at 0.45 K have too much thermal broadening for meaningful comparison with the predictions for critical-field locations and plateau rounding. However, because the critical field in this system is four times smaller than in $Na:Fe_6$, the possibility arises of a detailed experimental characterization of this curve over the first five plateaus.[6] Following the torque response to high fields [Fig. 8(b)] shows that the maximal value appears around the sixth plateau, and saturation occurs after the 25th.

V. DISCUSSION

The rigid-rotor model of Sec. II corresponds to the kinetic limit of a particle moving in a weak potential, and thus is quite suitable for the real Fe_6 and Fe_{10} systems where the anisotropy k_z is weak, and thus the barrier height is small. In addition to the energy levels and step positions discussed in Sec. III, the Hamiltonian (3) may be extended in second-order perturbation theory to give a qualitative description of the rounding of torque and magnetization plateaus. By contrast, the Lagrangean of Eq. (2) is most appropriate for the tight-binding limit of a particle in a strong potential and for

the semiclassical description of tunneling dynamics. This formulation gives a useful qualitative account of the energy-level splitting and of tunneling processes which result in plateau rounding, but is not applicable to the experimental curves at low temperatures. The numerical simulations remain the most reliable source of quantitative torque and magnetization data for the real system parameters.

With regard to the possibility of observing quantum coherent tunneling of the Néel vector in ferric wheel systems, we stress first that this is not possible in thermodynamic measurements of the type considered here. The unambiguous observation of quantum coherence requires measuring the evolution of the quantum state over several oscillation cycles without scattering into a different state, which necessitates time-resolved experiments and a discussion of decoherence. However, from the semiclassical formulation[4] one may estimate the parameters for quantum oscillations in the six- and 10-membered ring systems, using the parameters in Table I. The values of the tunnel splitting (the maxima in the sinusoidal function of B) are 11.4 K (235 GHz) for Na:Fe_6, 8.98 K (185 GHz) for Li:Fe_6, and 2.18 K (45 GHz) for Fe_{10}. These are very large values of the order of the barrier height and attempt frequency, implying the presence of very few (1 or 2) bound states in each potential minimum. However, because the resonance frequencies are so high, one may realistically expect to be able to observe a representative number of coherent oscillations within the decoherence time.

On the strength of the thermodynamic studies analyzed here, we may state that the magnetization and torque curves do appear to demonstrate that the desirable physical situation for quantum coherence[4] is realized. This consists of two, nearly degenerate, low-lying energy levels, suitably separated from higher levels and mixed by quantum (zero-point) transitions through a barrier (due to the easy-axis anisotropy) which separates them. However, we emphasize again that the key property of coherence cannot be shown only by thermodynamic measurements, such as magnetization. The experimental and theoretical aspects of this question have been addressed very recently for nuclear-magnetic-resonance and electron-spin-resonance probes by Meier and Loss.[12] A more extended analysis of the quantities (time-dependent correlation functions) which may be measured or computed analytically and numerically to provide additional insight into quantum coherence will be presented in a future publication.[13]

We conclude our analysis with a brief discussion of its relation to experiment. The existence of magnetization and torque steps, their locations for different field geometries and their heights are in good agreement with torque magnetometry results obtained[5] for Fe_6 and Fe_{10} samples at temperatures of 0.45 K. We stress again that the simulations for the minimal model of Eq. (10) show a vertical step at the appropriate critical field for all field angles. However, the recent, highly accurate results obtained[6] for the first torque step in Na:Fe_6 at temperatures down to 30 mK show two important features not reproduced by simulations of the model. One is the linear torque response observed for the $S=0$ plateau, and the other a temperature-independent field broadening of the magnetization steps.

The first feature may be caused by admixtures of higher-spin states in the composition of the ground state, of either ''extrinsic,'' meaning crystal misalignment or twinning, or ''intrinsic'' origin, meaning additional interaction terms not contained in Eq. (10). More interesting still is the second feature. An intrinsic origin for this effect implies a term in the Hamiltonian permitting transitions of $\Delta S_z = \pm 1$. Such terms do not arise from biaxial anisotropy, particularly in a ring geometry. This in turn may indicate a possible role for superhyperfine interactions with proton spins on H sites neighboring the metallic ions. However, a study[14] of this interaction in Fe_{10} has found that its effects are too small by some orders of magnitude to explain the observed broadening. Similarly, hyperfine interactions with the Fe nuclear spins may be excluded because the natural abundance of ^{57}Fe, the only species with nonzero nuclear spin, is so low. The most realistic intrinsic possibility is that the step width represents the energy scale of intermolecular interactions, as any coupling between the moments of neighboring rings would broaden the magnetization response. The observed full width of the first step at 40 mK[6] is 0.4 T, which would correspond to an effective interaction of 0.14 K per Fe atom in each ring. While the possible contributions to such interactions are difficult to quantify, simple geometrical considerations based on the crystallographic structure[15] suggest that the long-range dipolar component could indeed be of this order. Independent of the exact mechanism, any intrinsic step broadening requires coupling of an individual ring to an external system, and so the broadening energy scale may be taken as an inverse decoherence time for the purposes of quantum coherence studies.

A candidate extrinsic origin[6] is that molecules at the crystal surface may have different lattice parameters due to solvent loss, and thus undergo transitions at different field values corresponding to altered interaction strengths J. This effect should lead to rather small tails in the distribution of critical fields compared to the bulk response. Crystal mosaicity presents a further extrinsic possibility for step broadening, in that molecules with different angles to the applied field undergo transitions at different critical fields. In this scenario, the full width of the broadened first step at 40 mK would correspond to a quasi-Gaussian angular distribution with a full width of 9.2°, a rather large number which should be readily falsifiable from x-ray structural data. A more detailed analysis of these possibilities is deferred until further experimental data emerge to clarify the issue of extrinsic or intrinsic origin.

VI. CONCLUSION

We have presented a detailed analysis of the magnetization and torque response of the molecular magnetic systems Fe_6 and Fe_{10}. The step structure with critical fields B_{cn} and the variation of B_{cn} with field angle to the ring plane are readily understood from low-spin subspaces of a rigid-rotor Hamiltonian with weak spin anisotropy. Numerical simulations of the minimal but fully quantum-mechanical model demonstrate clearly a vanishing step width, accompanied by a rounding of the plateau regions even at zero temperature. These features can be related to those zero-point transitions

permitted within this model when the system is close to magnetization steps, where energy levels of different spin states are in close proximity. The differences between simulation and experimental observation in Fe_6 (Ref. 6) demonstrate the need for additional physical considerations on the theoretical side and characterization of a wider range of samples on the experimental, with a view toward discerning those features truly intrinsic to the ferric wheel systems. The angular variation of the step and rounding effects which emerge from simulations and theory should be observable in the most accurate experiments currently possible.[6] These would be of particular interest in Fe_{10} and may be expected to verify that the ferric wheel systems in transverse magnetic fields represent good candidates for the observation by further, time-resolved measurements of quantum coherent tunneling of the Néel vector.

ACKNOWLEDGMENTS

We are indebted to M. Affronte, A. Cornia, and A. Jansen for invaluable discussions and provision of data. We are further grateful to D. Awschalom, F. Meier, D. Gatteschi, J. Harris, and R. Sessoli for helpful comments, and to the Swiss National Fund for financial support. B.N. acknowledges the generosity of the Treubelfonds, and the support of the Deutsche Forschungsgemeinschaft through SFB 484. X.W. and X.Z. acknowledge financial support from the University of Fribourg and the University of Neuchâtel. D.L. acknowledges support from Molnanomag HPRN-CT-1999-00012.

[1] D. Gatteschi, A. Caneschi, L. Pardi, and R. Sessoli, Science **265**, 1054 (1994).
[2] A. Cornia, M. Affronte, A.G.M. Jansen, G.L. Abbati, and D. Gatteschi, Angew. Chem. Int. Ed. Engl. **38**, 2264 (1999).
[3] D. Loss, D.P. DiVincenzo, and G. Grinstein, Phys. Rev. Lett. **69**, 3232 (1992).
[4] A. Chiolero and D. Loss, Phys. Rev. Lett. **80**, 169 (1998).
[5] A. Cornia, A.G.M. Jansen, and M. Affronte, Phys. Rev. B **60**, 12 177 (1999).
[6] A. Cornia, A. G. M. Jansen, and M. Affronte (unpublished).
[7] A. Bencini and D. Gatteschi, *EPR of Exchange-Coupled Systems* (Springer-Verlag, Berlin, 1990).
[8] J. Harris and D. Awschalom (private communication).
[9] M. Affronte, J.C. Lasjaunias, A. Caneschi, and A. Cornia, Phys. Rev. B **60**, 1161 (1999).
[10] M. Affronte, J.C. Lasjaunias, and A. Cornia, Eur. Phys. J. B **15**, 633 (1999).
[11] *Density-Matrix Renormalization–A New Numerical Method in Physics*, edited by I. Peschel, X. Wang, M. Kaulke, and K. Hallberg (Springer-Verlag, Berlin, 1999).
[12] F. Meier and D. Loss, cond-mat/0101073 (unpublished).
[13] F. Meier, B. Normand, and D. Loss (unpublished).
[14] A. Cornia, A. Fort, M.G. Pini, and A. Rettori, Europhys. Lett. **50**, 88 (2000).
[15] A. Caneschi, A. Cornia, A.C. Fabretti, S. Foner, D. Gatteschi, R. Grandi, and L. Schenetti, Chem.-Eur. J. **2**, 1379 (1996).